CrossMark

J. Fluid Mech. (2018), *vol.* 847, *pp.* 244–265. © Cambridge University Press 2018
doi:10.1017/jfm.2018.307

Reappraisal of the velocity derivative flatness factor in various turbulent flows

S. L. Tang[1,2,†], R. A. Antonia[3], L. Djenidi[3], L. Danaila[4] and Y. Zhou[1,2]

[1]Institute for Turbulence–Noise–Vibration Interaction and Control, Shenzhen Graduate School, Harbin Institute of Technology, Shenzhen 518055, PR China

[2]Digital Engineering Laboratory of Offshore Equipment, Shenzhen 518055, PR China

[3]School of Engineering, University of Newcastle, Newcastle NSW 2308, Australia

[4]CORIA, CNRS, UMR 6614, Université de Rouen Normandie, 76801 Saint Etienne du Rouvray, France

(Received 18 July 2017; revised 17 February 2018; accepted 5 April 2018; first published online 21 May 2018)

We first analytically show, starting with the Navier–Stokes equations, that the value of the derivative flatness is controlled by pressure diffusion of energy, viscous destructive effects and large-scale effects (decay and/or production). The latter two terms tend to zero when the Taylor-microscale Reynolds number Re_λ is sufficiently large. We argue that the pressure-diffusion term should also tend to a constant at large Re_λ. Available data for the velocity derivative flatness, F, in different turbulent flows are re-examined and interpreted in the light of the finite-Reynolds-number effect. It is found that F can differ from flow to flow at moderate Re_λ; for a given flow, F may also depend on the initial conditions. The data for F in various flows, e.g. along the axis in the far field of plane and circular jets, and grid turbulence, show that it approaches a constant, with a value slightly larger than 10, when Re_λ is sufficiently large. This behaviour for F is supported, at least qualitatively, by our analytical considerations. The constancy of F at large Re_λ violates the refined similarity hypothesis introduced by Kolmogorov (*J. Fluid Mech.*, vol. 13, 1962, pp. 82–85) to account for the intermittency of the energy dissipation rate. It is not, however, inconsistent with Kolmogorov's original similarity hypothesis (*Dokl. Akad. Nauk SSSR*, vol. 30, 1941, pp. 299–303), although we contend that the power-law relation $F \sim Re_\lambda^{\alpha_4}$ (Kolmogorov 1962), which is widely accepted in the literature, has in reality been almost invariably used to 'model' the finite-Reynolds-number effect for the laboratory data and has been strongly influenced by the weighting given to the atmospheric surface layer data. The inclusion of the latter data has misled previous investigations of how F varies with Re_λ.

Key words: homogeneous turbulence, isotropic turbulence, turbulence theory

1. Introduction

There is no doubt that the first two similarity hypotheses of Kolmogorov (1941*a*,*b*), widely known as K41, and Kolmogorov's (1962) refined similarity hypothesis, known as K62, which was introduced to account for the so-called 'internal intermittency', have had a huge impact on turbulence research. According to K41, small-scale

† Email address for correspondence: shunlin.tang88@gmail.com

https://doi.org/10.1017/jfm.2018.307 Published online by Cambridge University Press

statistics should adopt particular universal forms when the focus is on small scales or scales lying within the dissipative and inertial ranges. For example, the Kolmogorov-normalized one-dimensional velocity spectra $\phi_u^*(k_1^*)$ (the asterisk denotes normalization by the Kolmogorov length scale, $\eta = (\nu^3/\overline{\epsilon})^{1/4}$, where ν is the kinematic viscosity of the fluid, $\overline{\epsilon}$ is the mean turbulent energy dissipation rate, and the overbar denotes time averaging, and/or Kolmogorov velocity scale, $u_K = (\nu\overline{\epsilon})^{1/4}$) collapse in the high-wavenumber region (Saddoughi & Veeravalli 1994). Antonia, Djenidi & Danaila (2014) showed that this collapse is consistent with the Navier–Stokes (NS) equations and does not require the Reynolds number to be large, nor does it require local isotropy to be rigorously satisfied, i.e. the constraints imposed by K41 can be relaxed significantly.

For the velocity structure functions, the first similarity hypothesis of K41 predicts

$$\overline{(\delta u^*)^n} = f_{un}(r^*), \tag{1.1}$$

with the velocity increment $\delta u = u(x + r) - u(x)$ between two points separated by a distance r along x, the flow direction; f_{un} is a universal function when normalized by η and/or u_K for each value of n. When $r \to 0$, (1.1) leads to

$$S_n = \frac{\overline{(\partial u/\partial x)^n}}{\overline{(\partial u/\partial x)^2}^{n/2}} = \text{const.} \tag{1.2}$$

for each value of n at large Re_λ ($= u'\lambda/\nu$, where λ is the longitudinal Taylor microscale $u'/(\partial u/\partial x)'$ and a prime denotes a root-mean-square value). According to K41, the constant associated with each n should be universal.

Many studies have focused on the evolution of S_n with Re_λ, with the view to test K41 and K62. With few exceptions (Tabeling *et al.* 1996; Belin *et al.* 1997), there has been strong support for the argument that $|S_n|$ ($n \geqslant 3$) can increase continuously with Re_λ, *viz.*

$$|S_n| \sim Re_\lambda^{\alpha_n} \quad (\alpha > 0) \tag{1.3}$$

(see e.g. Gibson, Stegen & Williams 1970; Wyngaard & Tennekes 1970; Van Atta & Antonia 1980; Antonia, Chambers & Satyaprakash 1981; Antonia, Satyaprakash & Hussain 1982; Sreenivasan & Antonia 1997; Davidson 2004; Ishihara *et al.* 2007; Ishihara, Gotoh & Kaneda 2009; Wyngaard 2010). However, it appears now that not only are the small-scale statistics affected by Re_λ (this is the so-called finite-Reynolds-number (FRN) effect, which is inextricably linked with the large-scale forcing in a specific flow), but also the approach towards an asymptotic state as Re_λ increases differs from flow to flow (Thiesset, Antonia & Djenidi 2014; Antonia *et al.* 2015, 2017). These results strongly indicate that the Re_λ dependence of S_n should be revisited. In particular, this dependence should be assessed separately in each flow. Such attempts have already been initiated by Antonia *et al.* (2015) and Tang *et al.* (2015*a*,*b*), who, starting from the NS equations, developed the locally isotropic form of the transport equation for $\overline{\epsilon}$ in the following flows: grid turbulence; along the axis in the self-preserving far field of a round jet; along the centrelines of a fully developed channel flow; and the far wake of a circular cylinder. They further showed that, in each flow they considered, the transport equation for $\overline{\epsilon}$ can be expressed in the generic form

$$S_3 + 2\frac{G}{Re_\lambda} = \frac{C}{Re_\lambda}, \tag{1.4}$$

https://doi.org/10.1017/jfm.2018.307 Published online by Cambridge University Press

where G is the non-dimensional enstrophy destruction coefficient of $\bar{\epsilon}$ defined as

$$G = \overline{u^2}\,\frac{\overline{(\partial^2 u/\partial x^2)^2}}{\overline{(\partial u/\partial x)^2}^2}. \tag{1.5}$$

(Note that Batchelor & Townsend (1947) first derived (1.4) for grid turbulence.) It was also shown that the analytical expressions for C differ from flow to flow. Further, since $2G/Re_\lambda$ was found to be very nearly constant for $Re_\lambda \geqslant 70$–100, S_3 approaches what appears to be a universal constant (≈ 0.53) when Re_λ is sufficiently large, but the way this constant is approached is flow-dependent. In fact, Re_λ only needs to exceed approximately 300 for S_3 to be considered constant for all the experimental data in flows considered in the above studies and direct numerical simulations (DNS) of turbulence in a periodic box (Kerr 1985; Jimenez *et al.* 1993; Yeung & Zhou 1997; Gotoh, Fukayama & Nakano 2002; Yeung, Donzis & Sreenivasan 2005). A notable exception to this behaviour comes from the data by Ishihara *et al.* (2007) and Gauding (2014) for DNS of turbulence in a periodic box up to $Re_\lambda = 1131$. This inconsistency has been discussed in detail by Antonia *et al.* (2015); we will revisit this issue later (§ 3) when discussing results for S_4. For (1.1), Pearson & Antonia (2001) showed that $\overline{(\delta u^*)^2}$ collapses in the dissipative range over a large range of Re_λ ($40 < Re_\lambda < 4250$) while Antonia *et al.* (2015) showed that $S_{\delta u}$, the skewness of δu, *viz.* $S_{\delta u} = \overline{(\delta u)^3}/\overline{(\delta u)^2}^{3/2}$, becomes independent of Re_λ in the dissipative range when Re_λ is sufficiently large.

The existing evidence only verified the constancy of (1.2) (K41) for $n = 3$ and the Re_λ independence of (1.1) (K41) in the dissipative range for $n = 2$, 3. It now seems implausible that (1.1) and (1.2) will behave differently for $n > 3$ at least in the dissipative range. In a recent paper, Antonia *et al.* (2017) examined the variation of S_n with Re_λ, equation (1.2), up to $n = 6$, on the axis of a plane jet, and found that S_n for $n = 3$ to 6 is constant (by definition, $S_2 = 1$) over a range $500 < Re_\lambda < 1100$, implying that the FRN effect is no longer present beyond $Re_\lambda \approx 500$. The authors further examined $\overline{(\delta u^*)^n}$ ($n = 2$–6) for the plane jet data at $Re_\lambda = 550$, 696, 826, 914 and 1067, respectively, and found that there is relatively good collapse for all the structure functions at small r^* (dissipative range). They also pointed out that all these results associated with the dissipative range favour K41 over K62 and hence imply that intermittency-related corrections are not needed at large Re_λ.

The work reported above focused only on assessing the FRN effect on the behaviour of S_3 in several turbulent flows. To our knowledge, however, there has been no attempt to examine the FRN effect on S_4 separately in each flow. Accordingly, the present paper, which complements and extends our earlier examination of S_3 (Antonia *et al.* 2015) aims at filling this gap. It has two major objectives:

(i) In § 2, starting from the NS equations, we derive an expression for the derivative flatness factor S_4 and argue that S_4 should, like S_3, be bounded when Re_λ is sufficiently large.

(ii) In § 3, we examine critically the data for S_4, as reported in the literature and new experimental data, in the light of the FRN effect. It is plausible that, at low to moderate Re_λ, S_4, like S_3, differs from flow to flow and exhibits a Re_λ dependence until it approaches a constant when Re_λ is sufficiently large. This trend appears to be adequately corroborated by the laboratory data considered in this paper. Further, the reasons why the atmospheric surface layer (ASL) data should be discarded when testing K41 and K62 are discussed briefly at the end of § 3.

https://doi.org/10.1017/jfm.2018.307 Published online by Cambridge University Press

2. Theoretical considerations

Since the main interest of this paper is the behaviour of the flatness factor of the velocity derivative, an appropriate starting point is the transport equation for the third-order structure function (Hill 2001), tenable under the assumptions of local homogeneity and isotropy:

$$\underbrace{\partial_t D_{111}}_{\text{term 1}} + \underbrace{\left(\partial_r + \frac{2}{r}\right) D_{1111}}_{\text{term 2}} - \underbrace{\frac{6}{r} D_{1122}}_{\text{term 2}'} = \underbrace{-T_{111}}_{\text{term 3}} + \underbrace{2\nu C}_{\text{term 4}} - \underbrace{2\nu Z_{111}}_{\text{term 5}}, \tag{2.1}$$

with $\partial_r \equiv \partial/\partial r$,

$$\left.\begin{aligned} D_{111} &= \overline{(\delta u)^3}, \\ D_{1111} &= \overline{(\delta u)^4}, \\ D_{1122} &= \overline{(\delta u)^2 (\delta v)^2}, \\ C(r,t) &= -\frac{4}{r^2} D_{111}(r,t) + \frac{4}{r} \partial_r D_{111} + \partial_r \partial_r D_{111}, \\ Z_{111} &= 3\,\overline{\delta u \left[\left(\frac{\partial u}{\partial x_l}\right)^2 + \left(\frac{\partial u'}{\partial x_l'}\right)^2 \right]}, \end{aligned}\right\} \tag{2.2}$$

where double indices indicate summation and a prime denotes variables at point $x + r$. Finally,

$$T_{111} = 3\,\overline{(\delta u)^2 \delta \left(\frac{\partial p}{\partial x}\right)}. \tag{2.3}$$

Terms 1 to 5 denote terms in (2.1). The next step is to consider the limiting form of these terms, for $r \to 0$, by applying a Taylor series expansion up to the fifth order in r. Because of homogeneity,

$$\frac{\partial}{\partial x} \overline{\left(\frac{\partial u}{\partial x}\right)^2 \left(\frac{\partial^2 u}{\partial x^2}\right)} \equiv 0 \quad \Rightarrow \quad 2\,\overline{\frac{\partial u}{\partial x}\left(\frac{\partial^2 u}{\partial x^2}\right)^2} = -\overline{\left(\frac{\partial u}{\partial x}\right)^2 \left(\frac{\partial^3 u}{\partial x^3}\right)}, \tag{2.4}$$

and hence

$$\overline{(\delta u)^3} \simeq \overline{\left(\frac{\partial u}{\partial x}\right)^3} r^3 - \frac{1}{4}\overline{\frac{\partial u}{\partial x}\left(\frac{\partial^2 u}{\partial x^2}\right)^2} r^5 + \cdots. \tag{2.5}$$

The fourth-order structure function can be written as

$$D_{1111} = \overline{(\delta u)^4} \simeq \overline{\left(\frac{\partial u}{\partial x}\right)^4} r^4 + \cdots \tag{2.6}$$

and similarly

$$D_{1122} = \overline{(\delta u)^2 (\delta v)^2} \simeq \overline{\left(\frac{\partial u}{\partial x}\right)^2 \left(\frac{\partial v}{\partial x}\right)^2} r^4 + \cdots. \tag{2.7}$$

https://doi.org/10.1017/jfm.2018.307 Published online by Cambridge University Press

An equation for S_4, the velocity derivative flatness factor, can be obtained by applying the following operator O, defined as

$$O \equiv \lim_{r\to 0} \frac{\overline{\dfrac{\text{terms in (2.1)}}{r^3}}}{\dfrac{\overline{(\delta u)^2}^2}{r^4}} = \lim_{r\to 0} r \cdot \frac{\text{terms in (2.1)}}{\overline{(\delta u)^2}^2}. \tag{2.8}$$

Term 1 in (2.1) represents a large-scale effect. It is written here as the temporal decay of $\overline{(\delta u)^3}$, but more general forms may include a production of $\overline{(\delta u)^3}$. For convenience, this term will be called $LS(r)$ ('large scale'), which can be written as

$$LS(r) = \frac{\partial}{\partial t}\overline{(\delta u)^3} = \left(\frac{\partial}{\partial t}u_K^3\right)\left(\frac{\overline{(\delta u)^3}}{u_K^3}\right) - u_K^3\frac{\partial}{\partial r^*}(\overline{(\delta u^*)^3})r^*\frac{1}{\eta}\frac{\mathrm{d}\eta}{\mathrm{d}t}. \tag{2.9}$$

We recall that, for decaying homogeneous and isotropic turbulence (HIT), the transport equation for the total kinetic energy $\overline{q^2}$ $(=\overline{u^2}+\overline{v^2}+\overline{w^2})$ is given by

$$\frac{1}{2}\frac{\partial \overline{q^2}}{\partial t} + \bar{\epsilon} = 0, \tag{2.10}$$

and $\overline{q^2}$ evolves in a power-law form during the decay, *viz.*

$$\overline{q^2} \sim t^n, \tag{2.11}$$

where n is the decaying exponent of the total kinetic energy. After substituting (2.11) in (2.10), we can obtain $\bar{\epsilon} \sim t^{n-1}$. Further, using the definitions of Re_λ, η and u_K leads to

$$\left.\begin{aligned} Re_\lambda &\sim t^{n/2+1/2}, \\ \eta &\sim t^{(-n+1)/4}, \\ u_K &\sim t^{(n-1)/4}. \end{aligned}\right\} \tag{2.12}$$

After substituting (2.12) in (2.9), the large-scale term can be written as

$$\begin{aligned} O(LS) &= \lim_{r\to 0}\left(r\frac{LS}{\overline{(\delta u)^2}^2}\right) = \lim_{r\to 0}\left(r\frac{(\partial/\partial t)\overline{(\delta u)^3}}{\overline{(\delta u)^2}^{3/2}\overline{(\delta u)^2}^{1/2}}\right) \\ &= \left(\frac{1-n}{2}\sqrt{\frac{15}{-n}} + 10\frac{(1-n)}{-n}\right)\frac{S_3}{Re_\lambda}. \end{aligned} \tag{2.13}$$

Because (i) the skewness of the velocity derivative, S_3, is bounded (Antonia *et al.* 2015), and (ii) n is finite with a value typically in the range -1.5 to -1.1 (e.g. Sinhuber, Bodenschatz & Bewley 2015), the $O(LS)$ term will be increasingly less important as Re_λ increases.

It is straightforward to show that $O(\text{term } 2) = S_4$ (because the operator O was designed with this in mind). Similarly, $O(\text{term } 2') = \overline{(\partial u/\partial x)^2(\partial v/\partial x)^2}/\,\overline{(\partial u/\partial x)^2}^2$. For simplicity, we introduce $S_{uv,2} = \overline{(\partial u/\partial x)^2(\partial v/\partial x)^2}/\,\overline{(\partial u/\partial x)^2}^2$.

https://doi.org/10.1017/jfm.2018.307 Published online by Cambridge University Press

β_1	β_2	β_3	β_4
750	−2000	500	$-1.1\left(\frac{1-n}{2}\sqrt{\frac{15}{-n}}+10\frac{(1-n)}{-n}\right)$

TABLE 1. Expressions and values for β_i in (2.15).

The pressure term becomes, once O is applied,

$$O(\text{term } 3) = -\frac{3\overline{\left(\frac{\partial u}{\partial x}\right)^2\frac{\partial^2 p}{\partial x^2}}}{\overline{\left(\frac{\partial u}{\partial x}\right)^2}^2} = -3\times 15^2\,\overline{\left(\frac{\partial u^*}{\partial x^*}\right)^2\left(\frac{\partial^2 p^*}{\partial x^{*2}}\right)}. \tag{2.14}$$

After applying the operator O, term 4 leads to $-18\times 15^2\,\overline{(\partial u^*/\partial x^*)(\partial^2 u^*/\partial x^{*2})^2}$, or, equivalently, $9\times 15^2\,\overline{(\partial u^*/\partial x^*)^2(\partial^3 u^*/\partial x^{*3})}$. Term 5 leads to a linear combination of $15^2\,\overline{(\partial^3 u^*/\partial x^{*3})(\partial u^*/\partial x^*)^2}$ and $2\times 15^2\,\overline{(\partial^3 u^*/\partial x^{*3})(\partial u^*/\partial y^*)^2}$. Since Djenidi *et al.* (2017*b*) showed that $S_{uv,2}\approx 0.85S_4$ (using DNS data for HIT), the limiting form of (2.1) as $r\to 0$ can be finally expressed as

$$S_4+\beta_1\overline{\left(\frac{\partial u^*}{\partial x^*}\right)^2\left(\frac{\partial^2 p^*}{\partial x^{*2}}\right)}+\beta_2\overline{\left(\frac{\partial^3 u^*}{\partial x^{*3}}\right)\left(\frac{\partial u^*}{\partial x^*}\right)^2}+\beta_3\overline{\left(\frac{\partial^3 u^*}{\partial x^{*3}}\right)\left(\frac{\partial u^*}{\partial y^*}\right)^2}=\beta_4\frac{S_3}{Re_\lambda}, \tag{2.15}$$

where β_i are dimensionless constants; the expressions and values for β_i are shown in table 1. Equation (2.15) is the most general expression for the derivative flatness factor, as only local homogeneity and isotropy have been assumed. Note that Djenidi *et al.* (2017*b*) have derived a similar equation for S_4 (see their equation (8)). However, the present (2.15) is more general and rigorous than their equation (8) for two reasons. First, they assume the flow is self-preserving; whilst it is relatively straightforward to show that the NS equations comply with this assumption (e.g. Antonia *et al.* 2014), it is best to avoid it altogether (note that this assumption was not used when testing the dependence of S_3 on Re_λ (see Antonia *et al.* 2015)). Second, for their equation (8), there is an inconsistency when using scaling variables since S_4 and $S_{uv,2}$ are normalized by Kolmogorov variables whereas the other quantities are normalized by u' and λ. Antonia *et al.* (2014) and Djenidi, Antonia & Danaila (2017*a*) have already shown, by using the NS equations, that the Kolmogorov variables are the correct scaling parameters for the small-scale quantities, i.e. all terms in equation (8) of Djenidi *et al.* (2017*b*) should have been normalized by Kolmogorov variables, as in (2.15).

We can rewrite (2.15) in a generic form as

$$S_4+\gamma=\beta\frac{S_3}{Re_\lambda}, \tag{2.16}$$

where

$$\gamma\equiv\beta_1\overline{(\partial u^*/\partial x^*)^2(\partial^2 p^*/\partial x^{*2})}+\beta_2\overline{(\partial^3 u^*/\partial x^{*3})(\partial u^*/\partial x^*)^2}+\beta_3\overline{(\partial^3 u^*/\partial x^{*3})(\partial u^*/\partial y^*)^2}.$$

https://doi.org/10.1017/jfm.2018.307 Published online by Cambridge University Press

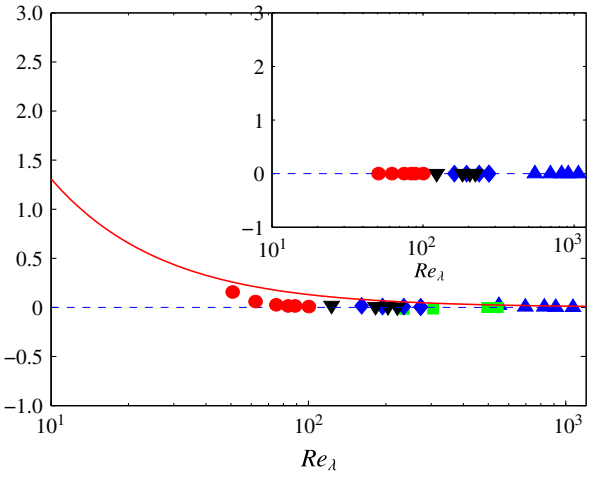

FIGURE 1. (Colour online) Dependence of $\beta_2\overline{(\partial^3 u^*/\partial x^{*3})(\partial u^*/\partial x^*)^2}$ (symbols) on Re_λ in various flows: grid turbulence, ● (Zhou & Antonia 2000); wakes, ◆ and ▼ correspond to data in wakes generated by two different initial conditions, namely a solid circular cylinder and a screen strip (Antonia, Zhou & Romano 2002); circular jet centreline, ■ (Xu, Antonia & Rajagopalan 2001); plane jet, ▲ (Zhou, Antonia & Chua 2005). The inset shows the magnitude of $\beta_3\overline{(\partial^3 u^*/\partial x^{*3})(\partial u^*/\partial y^*)^2}$. Also shown is the large-scale term (red curve, right-hand side of (2.16)) ($n = 1.2$). The blue dashed line corresponds to the value of 0.

For convenience, we have replaced β_4 by β. Equation (2.15) provides important insight into the physical mechanisms that affect the magnitude of the velocity derivative flatness factor S_4: (i) The term on the right, which represents the large-scale contribution, contains S_3, since it stems from term 1 in (2.1). It can be interpreted as the rate of change of the skewness (or rate of vortex stretching). (ii) The second term on the left represents the pressure diffusion while the third and fourth terms represent viscous destruction. The magnitude of S_4 can be considered to be controlled by the balance between the decay and/or production of the skewness, the pressure diffusion of energy (the second term on the left of (2.15)) and viscous/destructive effects (the third and fourth terms on the left of (2.15)). Figure 1 shows the dependence of the viscous/destructive effect term $\beta_2\overline{(\partial^3 u^*/\partial x^{*3})(\partial u^*/\partial x^*)^2}$ (symbols) on Re_λ in various flows; the inset shows the viscous/destructive term $\beta_3\overline{(\partial^3 u^*/\partial x^{*3})(\partial u^*/\partial y^*)^2}$. Also shown in figure 1 is the large-scale term (red curve) with $n = 1.2$. It can be seen that the viscous/destructive effect terms approach zero quickly whereas the large-scale term deceases gradually as Re_λ increases. Namely, the contribution of the viscous/destructive term is negligible at relatively small Re_λ. To our knowledge, no DNS estimates for the pressure-diffusion term in (2.15) are available. Application of the Cauchy–Schwarz theorem to this term yields

$$\left|\overline{\left(\frac{\partial u}{\partial x}\right)^2 \frac{\partial^2 p}{\partial x^2}}\right| \leqslant \overline{\left(\frac{\partial u}{\partial x}\right)^4}^{1/2} \overline{\left(\frac{\partial^2 p}{\partial x^2}\right)^2}^{1/2}, \tag{2.17}$$

https://doi.org/10.1017/jfm.2018.307 Published online by Cambridge University Press

which finally leads to

$$\left|\overline{\left(\frac{\partial u^*}{\partial x^*}\right)^2\left(\frac{\partial^2 p^*}{\partial x^{*2}}\right)}\right| \leqslant S_4^{1/2}\left(\int_0^\infty k^{*4}E_p^*(k^*)\,\mathrm{d}k^*\right)^{1/2}, \tag{2.18}$$

where $E_p(k)$ is the three-dimensional pressure spectrum. Therefore, when Re_λ is sufficiently large (the viscous/destructive and large-scale terms will become negligible), equation (2.16) can be written as

$$S_4 \approx \left|\beta_1\overline{\left(\frac{\partial u^*}{\partial x^*}\right)^2\left(\frac{\partial^2 p^*}{\partial x^{*2}}\right)}\right| \leqslant \beta_1 S_4^{1/2}\left(\int_0^\infty k^{*4}E_p^*(k^*)\,\mathrm{d}k^*\right)^{1/2} \tag{2.19}$$

or

$$S_4^{1/2} \leqslant \left(\int_0^\infty k^{*4}E_p^*(k^*)\,\mathrm{d}k^*\right)^{1/2}. \tag{2.20}$$

Djenidi *et al.* (2017*b*) inferred, on the basis of the DNS results of Ishihara *et al.* (2003), that this integral tends to a constant for sufficiently large Reynolds numbers, implying that S_4 should be bounded when Re_λ is sufficiently large. An increased rate of local vortex stretching leads to an increased concentration of turbulent fluctuations in reduced regions of space, and hence an increased intermittency and larger skewness and flatness factors. The pressure diffusion term accounts for non-local interactions. It represents the correlation between the fluctuating local energy dissipation rate and one component of the Laplacian of the pressure fluctuation. The physical interpretation of (1.4) is now well understood: viscous effects act to limit the final value of S_3 once Re_λ is sufficiently large (i.e. when C/Re_λ is negligible). One can similarly argue that the flatness factor S_4, as given by (2.15), is expected to become constant when Re_λ is sufficiently large, i.e. the enhancement of 'intermittency' must be halted by the effect of both pressure diffusion and viscous terms on the left-hand side of (2.15). As the Reynolds number increases, the decay and/or production of the skewness as well as the viscous destruction decrease gradually before disappearing altogether, leaving only the pressure diffusion to balance S_4. Gotoh & Nakano (2003) discussed the role of the pressure diffusion by examining the transport equation for S_n ($n = 4$, 6 and 8) using DNS data. They proposed a model for the pressure diffusion, based on Bernoulli's equation, and argued that the pressure gradient acts to resist vortex stretching, thus limiting the level of intermittency. We recall that Kraichnan (1991) had pointed to the possibility that pressure forces can attenuate the intermittency, leading to universal statistics of dissipation range scales.

The interplay between the different physical mechanisms described above is conceptually analogous to the fact that the skewness of the derivative (again, for large Reynolds numbers) is only balanced by the viscous destruction of the second-order moments (or energy), as reflected by (1.4). Reasoning by 'induction' would lead to the expectation that the nth-order moments of the velocity derivative are balanced mainly by the viscous destruction of the $(n-1)$th-order moments. In § 3, we further examine the main outcome of this section, i.e. (2.15) or (2.16), using experimental data for S_4; naturally, we recognize that (2.15) can only be tested realistically once reliable DNS estimates of the pressure-diffusion term become available.

https://doi.org/10.1017/jfm.2018.307 Published online by Cambridge University Press

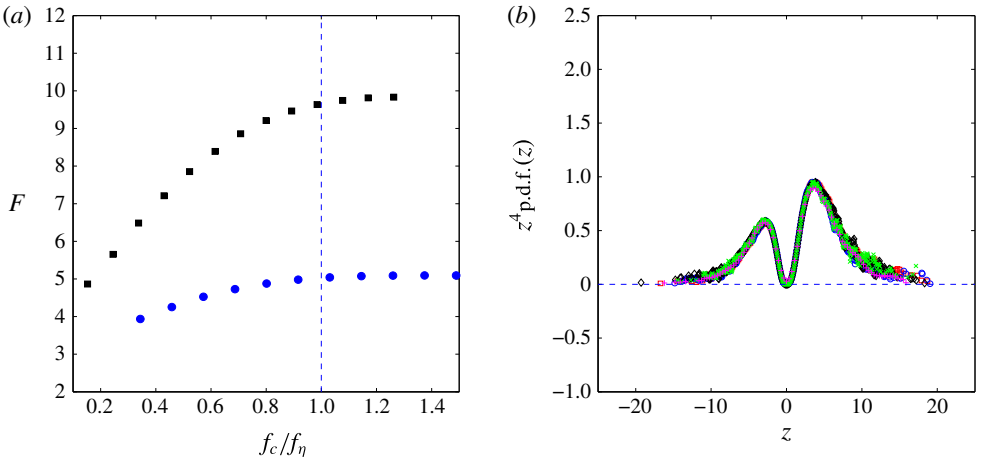

FIGURE 2. (Colour online) (*a*) Dependence of F on f_c/f_η for the plane jet data at $Re_\lambda = 550$ (■; Zhou *et al.* 2005) and the channel flow data at $Re_\lambda = 36$ (●; Tang *et al.* 2015*a*). The vertical dashed line corresponds to $f_c/f_\eta = 1$. (*b*) The probability density function (p.d.f.) of z multiplied by z^4 along the axis of the plane jet with $Re_\lambda = 550$ (black), 696 (blue), 826 (red), 914 (pink) and 1067 (green) (Zhou *et al.* 2005). The dashed line indicates the value of 0.

3. Results for S_4

3.1. *Measurement of* S_4

Difficulties in measuring small-scale quantities such as S_4 (often denoted by F in the literature; we will hereafter use F and S_4 interchangeably) have been discussed in detail by Antonia *et al.* (1982). Therefore, before discussing the results, it is important to comment on the accuracy of the measurements of F (Zhou & Antonia 2000; Pearson & Antonia 2001; Antonia *et al.* 2002; Zhou *et al.* 2005; Tang *et al.* 2015*a*) that are used here. There are three major 'systematic' error sources when measuring F: the uncertainty associated with the spatial/time resolutions of the hot wire, and the duration of the recorded signal. As an example, for the plane jet data, the spatial resolution of the wire is adequate even at the largest Re_λ (= 1109; Pearson & Antonia 2001) due to the fact that the wire diameter is 1.27 μm (the wire length is $\sim 3.1\eta$). In fact, for a single hot-wire measurement, the magnitude of F is mainly affected by the temporal resolution and is practically insensitive to the spatial resolution (Burattini, Lavoie & Antonia (2008) demonstrated this in the context of S_3). Figure 2(*a*) shows that the magnitude of F increases with f_c/f_η (f_c and $f_\eta = U/2\pi\eta$ are the filter cutoff frequency and the Kolmogorov frequency, respectively), approximately reaches a maximum at $f_c/f_\eta \approx 1.0$ and remains constant at higher frequencies. For most of our data, f_c was chosen close to or slightly larger than the Kolmogorov frequency f_η (i.e. $f_c/f_\eta \geqslant 1$), which is adequate for estimating F (see figure 2*a*). The final choice of f_c was dictated by the onset of the electronic noise in the anemometer circuit. The record duration is also adequate since both z^2 p.d.f.(z) and z^4 p.d.f.(z) go to zero at large $|z|$ (figure 2*b*). There remains the possibility of a random error associated mainly with the propagation of errors due mostly to the measurement of u. An estimate was obtained from three single wires in the vorticity probe and shown

https://doi.org/10.1017/jfm.2018.307 Published online by Cambridge University Press

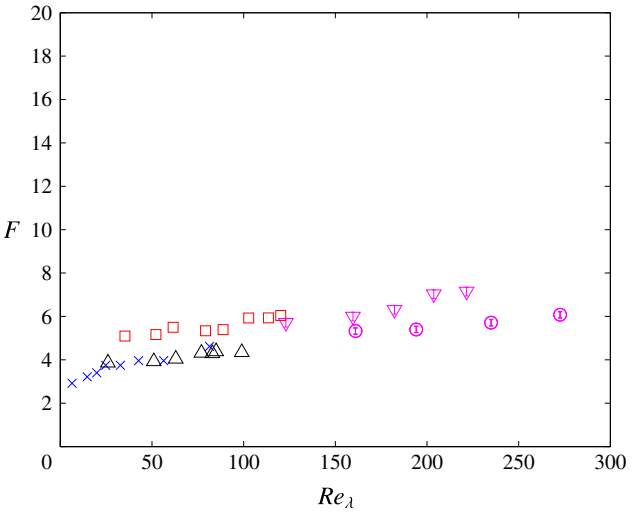

FIGURE 3. (Colour online) Distributions of F for various flows at relatively low Re_λ. Centreline of a fully developed channel flow: □, estimated from the data of Tang *et al.* (2015*a*). SFPBT: ×, Kerr (1985). Grid turbulence: △, estimated from the data of Zhou & Antonia (2000). Wakes: ○ and ▽ correspond to data in wakes generated by two different initial conditions, namely a solid circular cylinder and a screen strip, estimated from the data of Antonia *et al.* (2002). The error bars for wake data are also shown; note that they are very small. To facilitate visual comparison with data in other flows, the ordinate scale used in this figure is the same as that in figures 4, 5, 6, 7 and 8(*b*).

as error bars in figures 3 and 4 for the data of Antonia *et al.* (2002) and Zhou *et al.* (2005).

3.2. *Velocity derivative flatness F at relatively small Re_λ*

Antonia *et al.* (2015) showed that, although S_3 approaches a constant when Re_λ is sufficiently large, the magnitude of S_3 is flow-dependent when Re_λ is small or moderate. There is no *a priori* reason why S_4 should behave differently than S_3 when Re_λ varies. The similarity between (1.4) and (2.16) suggests that S_4 should also depend on the type of flow at small to moderate Re_λ. To verify this, we report (figure 3) values of F in various turbulent flows at relatively small Re_λ, e.g. grid turbulence, along the centreline of a fully developed channel flow, and 'stationary' forced periodic box turbulence (SFPBT) at relatively low Re_λ. In these flows, local isotropy (LI), which is a key ingredient of K41 and K62, is satisfied closely (see Antonia *et al.* 2015; Tang *et al.* 2015*a*,*b*); along the axis in the far field of a plane jet, LI is also satisfied closely (Antonia *et al.* 2017). The data show a clear trend: F increases as Re_λ increases for all the flows considered. The magnitude of F is larger along the channel centreline than for either grid turbulence or SFPBT. Note that the distributions of F obtained in two different grid turbulence experiments agree well over the same Re_λ range. Also included in figure 3 are the data in wakes generated by two different initial conditions: a solid circular cylinder and screen strip; they are estimated from the data of Antonia *et al.* (2002). Thiesset, Danaila & Antonia (2013) used the same wake data to assess LI through the isotropic relation between second-order structure functions of the lateral and longitudinal velocity increments,

https://doi.org/10.1017/jfm.2018.307 Published online by Cambridge University Press

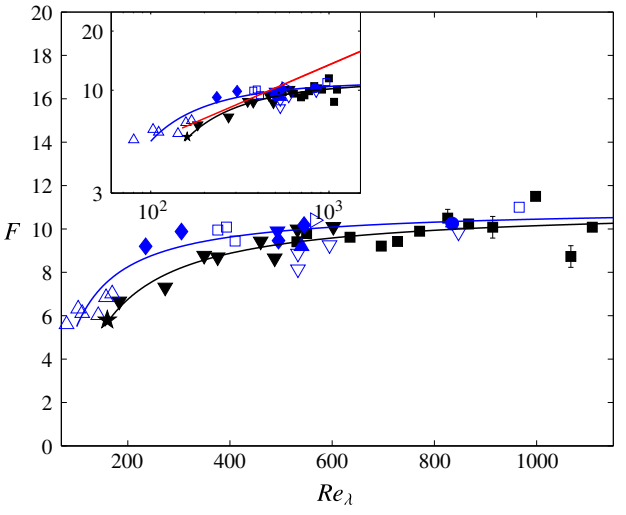

FIGURE 4. (Colour online) Dependence of F on Re_λ in two types of flows and qualitative comparison with (2.16). Plane jet: ★, Antonia, Anselmet & Chambers (1986); ▼ (black), Sreenivasan & Antonia (1997); ■, Antonia *et al.* (2017), without identifying the data sources. Circular jet: △, Mi, Xu & Zhou (2013); ◆, Xu *et al.* (2001); ●, Kahalerras, Malecot & Gagne (1998); ▼ (blue), Pearson & Antonia (2001); ▲, Friehe, Atta & Gibson (1971); ▽, Kuo & Corrsin (1971); □, Antonia *et al.* (1981) (see also Antonia *et al.* 1982); ▷, Burattini (private communication). The blue and black curves are least-squares fits with (2.16), corresponding to circular jet ($\gamma = -11$ and $\beta = 1000$) and plane jet ($\gamma = -11$ and $\beta = 1600$), respectively. The inset shows all the data using log–log coordinates. Also shown in the inset is the K62 prediction (red curve): $F = 0.91 Re_\lambda^{0.39}$ (Gylfason, Ayyalasomayajula & Warhaft 2004).

viz.

$$\overline{(\delta v)^2}_{iso} = \left(1 + \frac{r}{2}\frac{\mathrm{d}}{\mathrm{d}r}\right)\overline{(\delta u)^2}. \tag{3.1}$$

They showed that (3.1) is satisfied in the dissipative range ($r^* < 20$), although the range of separations over which (3.1) is satisfied depends on the initial conditions. Figure 3, which shows that F is multivalued, suggests that F can, for a given flow, depend on the initial conditions. It can also vary from flow to flow.

3.3. *Derivative flatness factor S_4 at large Re_λ*

We now consider data for S_4 obtained by various authors in a wide range of flows. Separate plots are used (figures 4, 6, 7 and 8*b*), with the same ordinate scale. We note that almost all the previous assessments of the Re_λ dependence of F have included the high-Re_λ ASL data and led to the observation that $F \sim Re_\lambda^{\alpha_4}$ (K62), e.g. figure 6 of Sreenivasan & Antonia (1997). For reasons that will be discussed in detail later (in the context of figure 8*a*), we have excluded the ASL data from figures 4, 6, 7 and 8(*b*).

Recently, Antonia *et al.* (2017) showed that, along the axis of the far field of a plane jet, F is practically constant over a range of Re_λ ($500 < Re_\lambda < 1100$) for several datasets, which are reproduced in figure 4 without identifying the data sources. Also included in figure 4 are the data of Antonia *et al.* (1986) and Sreenivasan & Antonia (1997) also for the plane jet at lower Re_λ. In order to examine the boundedness of F,

https://doi.org/10.1017/jfm.2018.307 Published online by Cambridge University Press

we have added in figure 4 data obtained along the axis of the far field of a circular jet (Friehe *et al.* 1971; Kuo & Corrsin 1971; Antonia *et al.* 1981, 1982; Kahalerras *et al.* 1998; Pearson & Antonia 2001; Xu *et al.* 2001; Mi *et al.* 2013). Antonia *et al.* (1982) measured F on the centreline of a circular jet at $x/d = 70$, 80, 90 and 120 at a fixed Re_d ($= U_j d/\nu = 55\,600$, where U_j is the jet exit velocity and d the nozzle diameter) on the jet axis (see their figure 7) and showed that F is approximately constant (≈ 10) at $x/d = 80$, 90 and 120, respectively, which would be consistent with self-preservation at least for the small scales, and is also in good agreement with other data at comparable Re_λ in this flow (see figure 4). Their magnitude of F at $x/d = 70$ (≈ 8.4) appears to be underestimated, compared to F for $x/d > 70$. For this reason, this data point is not shown in figure 4.

Equation (1.4) allows the FRN effect on S_3 to be estimated quantitatively in various flows, i.e. it allows an analytical prediction for S_3. Evidently, it would be desirable to investigate the FRN effect on F with (2.16) in each flow. However, the estimation of γ involves the simultaneous measurement of pressure and velocity fluctuations. Unfortunately, these quantities are not yet available and we only know the constant for β in decaying HIT. Thus, we cannot predict F analytically. However, in order to highlight the Re_λ dependence of F, we apply a least-squares fit based on (2.16) to the data reported in figure 4; we assume that γ and β are constants with the expectation that β should vary between different flows to reflect the difference of FRN effect in each flow. As mentioned in the introduction, S_3 appears to reach the same constant value (≈ -0.53) when $Re_\lambda \geqslant 300$; further, for Re_λ in the range 100–300, S_3 changes by less than 20 % in different flows (Antonia *et al.* 2017). We have therefore chosen $S_3 \approx -0.53$ for curve fitting to these two flows. The fitted curves are shown in figure 4. The following comments can be made.

(i) The data in these two flows can be reasonably fitted with (2.16), with the same value of γ ($= -11$) but different values of β (1000 for the circular jet and 1600 for the plane jet, respectively).

(ii) The fitted curves show the same trend as the data: the flow dependence when Re_λ is small to moderate (< 600) becomes smaller when $Re_\lambda \geqslant 600$.

(iii) The trend shown by the data and the curves is clear: F appears to approach a limiting value, possibly slightly smaller than 12, when Re_λ is sufficiently large. In general, Re_λ needs to exceed approximately 500 for F to be considered constant in these two flows. The way this constant is approached is flow-dependent.

(iv) The larger β, the slower the rate at which the final value is reached. Evidently, the approach is slower on the axis of the plane jet ($\beta = 1600$) than on the axis of the circular jet ($\beta = 1000$).

The constancy of F at large Re_λ is consistent with the analytical prediction of Qian (1986), who used a closure theory, the analytical results of Djenidi *et al.* (2017*b*) and the prediction of K41. But it cannot be reconciled with K62, which predicts $F \sim Re_\lambda^{\alpha_4}$. This can be observed clearly from the inset of figure 4, which shows that K62 (as an example, we show a K62 prediction (red curve): $F = 0.91 Re_\lambda^{0.39}$ of Gylfason *et al.* (2004)) is not supported by the experimental data in both circular and plane jets. In fact, the K62 prediction is at best tangential to the plane jet data and does not represent at all the circular jet data. Since FRN-affected data (collected in different flows) as well as the ASL data (possibly also affected by the FRN effect) were included in almost all the previous examinations of F versus Re_λ, it is not surprising that a consensus has not been reached for the value of α_4. Indeed, the exponent α_4 can vary between 0.31 and 0.41 (e.g. Van Atta & Antonia 1980; Antonia *et al.* 1982;

https://doi.org/10.1017/jfm.2018.307 Published online by Cambridge University Press

Ishihara *et al.* 2007), depending on the intermittency models. The previous discussion leads to the conclusion that the difference in the values of α_4 reflects the difference in the way F is affected by the different large-scale motions.

The DNS data for F in SFPBT are shown figure 5. It can be seen from this figure that there is good collapse for all the DNS data when $Re_\lambda \leqslant 200$; the same can be observed for S_3 in the same flow; see figure 5 of Antonia *et al.* (2015). For $Re_\lambda > 200$, however, the two sets of data obtained by Ishihara *et al.* (2007) ($k^*_{max} = 2$ and $k^*_{max} = 1$, respectively) indicate that F increases as Re_λ increases (the Gotoh *et al.* (2002) data, for $k^*_{max} = 1$, give the impression that F has almost become constant at $Re_\lambda = 460$). The authors claim agreement with $F \sim Re_\lambda^{\alpha_4}$ ($\alpha_4 = 0.31$ (Hill 2002) and 0.39 (Gylfason *et al.* 2004), respectively, which have also been shown in the inset of figure 5), but in fact it is clear that the rate of increase of F with Re_λ decreases as Re_λ increases (see the linear plot) and the relation $F \sim Re_\lambda^{\alpha_4}$ does not really represent the trend of the Ishihara *et al.* (2007) data (see the log–log plot). We can only surmise that Ishihara *et al.*'s (2007) claim that $F \sim Re_\lambda^{\alpha_4}$ was influenced by the inclusion of the ASL data. We contend that their data do not exclude the possibility that it will approach a constant at large Re_λ. We have already commented (Antonia *et al.* 2015) on the behaviour of their Kolmogorov-normalized spectra, in particular the systematic increase of $k^{*4}E^*(k^*)$ (for $k^* > 0.5$) with Re_λ (Ishihara *et al.* 2007). This is not consistent with Kolmogorov scaling, as inferred from the NS equation (e.g. Antonia *et al.* 2014), nor is it consistent with the support for this scaling provided by previous DNS studies of forced periodic box turbulence (Jimenez *et al.* 1993; Yeung & Zhou 1997; Gotoh *et al.* 2002; Yeung *et al.* 2005), for Re_λ up to 700. As overwhelmingly supported by experimental data – and also the DNS data of Jimenez *et al.* (1993), Yeung & Zhou (1997), Gotoh *et al.* (2002, see figure 12 of their paper) and Yeung *et al.* (2005, up to $Re_\lambda \approx 700$, see figure 1 of their paper) (note that S_3 is constant for $Re_\lambda \approx 240$–700 whereas a proper '4/5' inertial range has yet to be established) – the FRN effect first disappears at the smallest scales and subsequently at increasingly larger scales as Re_λ increases. This is in contrast to the claim by Ishihara *et al.* (2007, 2009) that the Reynolds-number effect has 'nearly' disappeared in the so-called scaling range (in Ishihara *et al.* (2009), the scaling range exponents, which are independent of Re_λ, are inferred from Gotoh *et al.*'s (2002) data at $Re_\lambda = 460$) whereas S_3 and S_4 continue to increase. Further, Ishihara *et al.* (2009) conclude (their summary point number 3) that

> [t]he DNS data support the existence of a universal local equilibrium state at small scales in high Re in the manner of K41

and (their summary point number 5) that

> [. . .] with regard to the Re dependences of statistics, (i) some statistics such as the energy-dissipation rate, the normalized third-order structure function, and the energy-flux spectrum in the inertial subrange tend toward finite constants as $Re \to \infty$; (ii) others, such as the energy spectrum in the dissipation range, tend toward a form independent of Re in accordance with K41, but the approach may be very slow; and (iii) some statistics, such as the skewness and flatness factors of the velocity gradients and pressure gradients, have an algebraic dependence on Re_λ.

These conclusions imply that K41 and K62 may coexist, a possibility that is difficult to understand, at least in the context of the laboratory measurements and previous

https://doi.org/10.1017/jfm.2018.307 Published online by Cambridge University Press

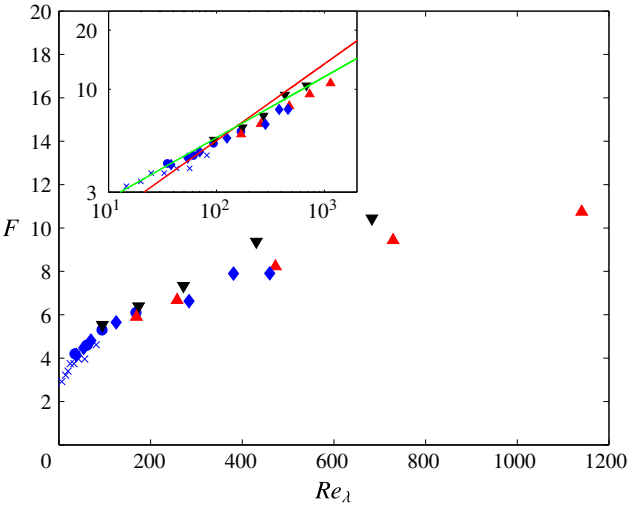

FIGURE 5. (Colour online) Dependence of F on Re_λ in SFPBT: $\times$, Kerr (1985); ▼ and ▲ correspond to $k^*_{max} = 2$ and $k^*_{max} = 1$, respectively, from Ishihara *et al.* (2007); ◆, Gotoh *et al.* (2002); ●, Wang *et al.* (1996). The inset shows all the data using log–log coordinates. Also shown in the inset is the K62 prediction: $F = 0.91Re_\lambda^{0.39}$ (red curve) (Gylfason *et al.* 2004) and $F = 1.36Re_\lambda^{0.31}$ (green curve) (Hill 2002); both predictions were used by Ishihara *et al.* (2007) (see their figure 6).

and earlier DNS results. Our observations indicate that the FRN effect first disappears in the dissipative range and lingers on in the scaling range, i.e. larger scales (in the scaling range) are more likely to continue to be affected by Re_λ than smaller scales (in the dissipative range). Evidently, Ishihara *et al.* (2007) do not share this view. To our knowledge, a plausible mechanism, which explains how intermittency, as expressed by F say, can continue to increase with Re_λ whilst the scaling range exponents are no longer affected by Re_λ (Ishihara *et al.* 2009), has yet to be proposed.

Tabeling *et al.* (1996) and Belin *et al.* (1997) reported various statistics for $\partial u/\partial x$ in helium gas at low temperature in a cylindrical container bounded by two counter-rotating disks over an impressively large range of Re_λ: 150–5040 (Tabeling *et al.* 1996) and 150–2300 (Belin *et al.* 1997). In the context of this paper, notwithstanding previous reservations (Sreenivasan 1995; Sreenivasan & Antonia 1997) concerning the characteristics of the sensor used in these experiments, these results are useful since the range of Re_λ is large enough to allow the assessment of the FRN effect on F with minimal ambiguity. As far as we are aware, there has been no systematic examination of LI in the central region of this flow. However, the isotropic form of the transport equation for $\overline{(\delta u)^2}$ is verified reasonably well (Moisy, Tabeling & Willaime 1999). Antonia *et al.* (2015) have already reported and discussed elsewhere the data for S_3, where S_3 remains constant ($\simeq -0.50$) over a range of Re_λ extending up to 2000. The data for F of Tabeling *et al.* (1996) and Belin *et al.* (1997) are shown in figure 6 for Re_λ up to 3000. The figure presents a similar trend to that of the data in figure 4: F increases with Re_λ for Re_λ up to approximately 700, and, allowing for the scatter, seems to be approximately constant beyond that value. There is a peak in F in the vicinity of $Re_\lambda \simeq 700$, which was speculated (by the authors) to correspond to a transition, possibly a 'mixing' transition as described by Dimotakis (2000) and also observed by Pearson & Krogstad (2001) in passive

https://doi.org/10.1017/jfm.2018.307 Published online by Cambridge University Press

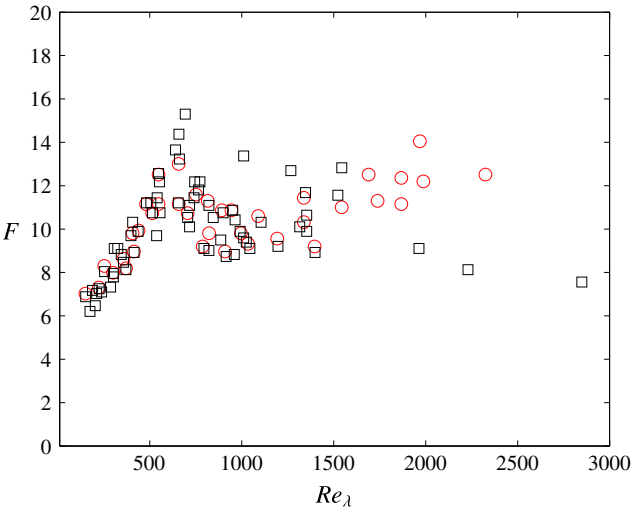

FIGURE 6. (Colour online) Dependence of F on Re_λ in flow between counter-rotating disks: ○, Tabeling *et al.* (1996); □, Belin *et al.* (1997).

grid turbulence, to a new state of turbulence (see the discussion of this transition in Tabeling & Willaime (2002)).

Gylfason *et al.* (2004) examined the Reynolds-number dependence of F in grid turbulence with and without mean shear ($Re_\lambda = 100$–1000). Here, we only show the data in grid turbulence without a mean shear since the latter has a significant effect on LI (Kim & Antonia 1993; Shen & Warhaft 2000) (see also Tang *et al.* (2016), who showed that the higher-order statistics depart more strongly from LI in sheared than in shearless grid turbulence); not surprisingly, the magnitude of F is increased, at the same Re_λ, relative to that measured without shear; also, F increases along distinctly different paths for the shearless and sheared cases. Gylfason *et al.*'s (2004) data (their figure 3) for shearless grid turbulence are reported in figure 7; note that only data for $l_w/\eta \leqslant 1.75$ are shown, as recommended by Gylfason *et al.* (2004). Also shown in this figure are data for grid turbulence collected from other published studies. Two comments can be made with regard to figure 7.

(i) All the data for F collapse reasonably well onto a single distribution, up to $Re_\lambda \simeq 730$. This distribution has the same behaviour as that observed in figure 4: for $Re_\lambda \leqslant 600$, the magnitude of F increases with Re_λ; for $Re_\lambda \geqslant 600$, F eventually reaches a constant, which is about the same as that measured by Kahalerras *et al.* (1998) at $Re_\lambda = 2500$. This trend is similar to that observed in figures 4 and 6. On the contrary, the inset of figure 7 shows that shearless grid turbulence data ($50 < Re_\lambda < 160$) from other published studies and especially the data point at $Re_\lambda = 2500$ are not adequately described by the relation $F = 0.91Re_\lambda^{0.39}$ (K62). Further, as discussed in the context of figures 4 and 5, Gylfason *et al.*'s relation $F = 0.91Re_\lambda^{0.39}$ cannot represent the data in other flows.

(ii) The data show that F approaches a constant whose magnitude is in approximate agreement with that in plane and circular jets when $Re_\lambda > 600$ (figure 4).

Figure 8(*a*) reproduces the compilation of F versus Re_λ by Sreenivasan & Antonia (1997) (their figure 6); we have drawn a 'red' line around the symbols corresponding

https://doi.org/10.1017/jfm.2018.307 Published online by Cambridge University Press

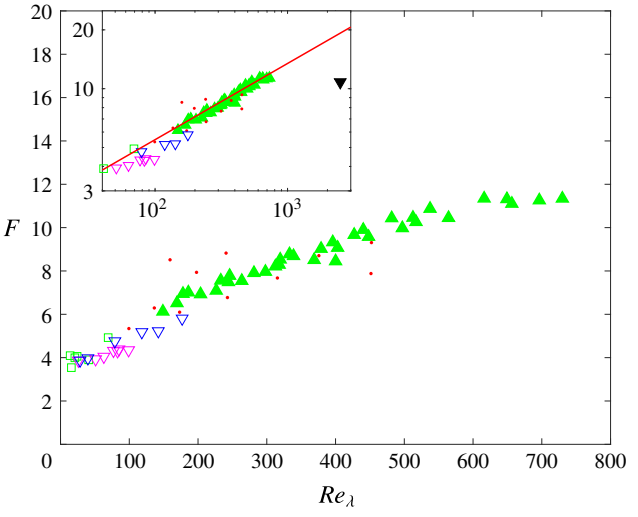

FIGURE 7. (Colour online) Dependence of F on Re_λ in shearless grid turbulence: □, Batchelor & Townsend (1947, 1949); ▽ (magenta), estimated from the data of Zhou & Antonia (2000) ($l_w/\eta = 0.6$–2.5); ▽ (blue), Tong & Warhaft (1994) ($l_w/\eta = 0.8$–1.3); ●, Mydlarski & Warhaft (1996) ($l_w/\eta = 1.8$–5.2); ▲ corresponds to the data from small and large tunnels, respectively, without mean shear, reproduced from figure 3 of Gylfason *et al.* (2004); note that only data for $l_w/\eta \leqslant 1.75$ are shown, as recommended by Gylfason *et al.* (2004). The inset shows all the data on a log–log plot. Also shown in the inset is one measurement ($F = 10.8$, ▼) of Kahalerras *et al.* (1998) along the axis of the ONERA wind tunnel (similar to grid turbulence) for $Re_\lambda = 2500$ and the K62 prediction (red curve): $F = 0.91 Re_\lambda^{0.39}$ (Gylfason *et al.* 2004).

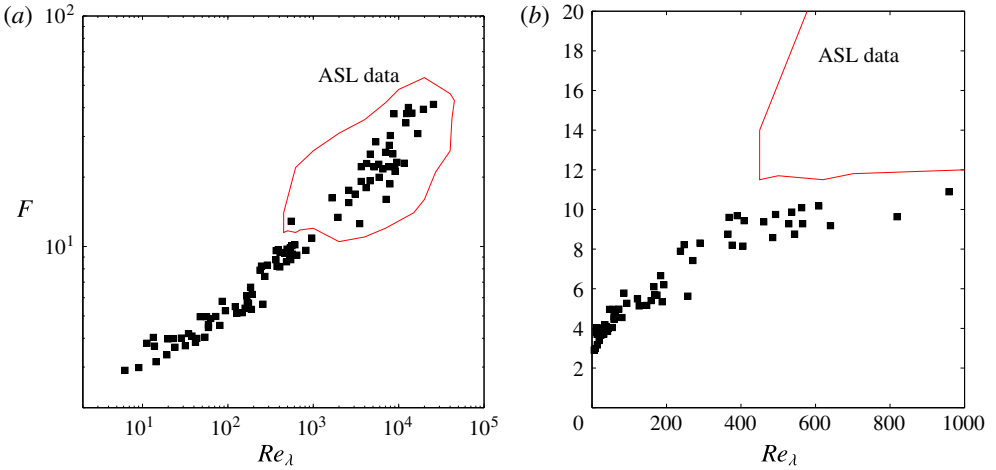

FIGURE 8. (Colour online) (*a*) Dependence of F on Re_λ reproduced (log–log plot) from figure 6 of Sreenivasan & Antonia (1997) without identifying the data sources. A 'red' line has been drawn around the ASL data to distinguish these from the other (laboratory) data. (*b*) An enlargement of the range for (laboratory) data using linear axes. Note the presentation in (*b*) is completely consistent with that in figures 4–7.

https://doi.org/10.1017/jfm.2018.307 Published online by Cambridge University Press

to the ASL data. In order to compare figure 8(*a*) with figures 3–7, an enlargement of the Re_λ range corresponding to the laboratory data in figure 8(*a*) is shown in figure 8(*b*) with linear scales instead of log scales (the vertical scale is identical to that used in figures 4–7). Antonia *et al.* (2017) carried out a similar comparison for S_3 and made the following points.

(i) Since the data affected by the FRN effect were included in the compilation for S_3, many values of the exponent α_3 in the power-law relation $S_3 \sim Re_\lambda^{\alpha_3}$ (K62) have been proposed.

(ii) The ASL data should not be used to test K41 and K62 because they were collected at relatively small heights (often below 30 m) above the ground or ocean surface where the requirements for K41 and K62 are unlikely to be met. Similar comments can be made for F on the basis of figures 3–8.

It can be seen from figure 8(*b*) that there is a fair amount of 'apparent' scatter in the laboratory data for $Re_\lambda \leqslant 600$. In fact, this scatter reflects, to a large extent, the systematic difference in how F approaches a constant in different flows, e.g. figure 3. In similar fashion to S_3 (Antonia *et al.* 2017), no attempt was made to distinguish between distributions of F in different flows.

Almost all the previous examinations of F versus Re_λ have included the high-Re_λ ASL data, e.g. figure 6 of Sreenivasan & Antonia (1997) (or the present figure 8*a*). The inclusion of the ASL data leads to a power-law dependence of F on Re_λ (K62) that is inconsistent with the results in figures 4, 6 and 7. We have excluded the ASL data from figures 4, 6 and 7 since Djenidi *et al.* (2017*c*) have provided several reasons why the ASL data should be discarded when testing K41 and K62. We discuss this further here, in some detail. The ASL data have been obtained in a flow region where the effects of the mean shear and proximity to the surface (which causes blockage effects to arise) cannot be ignored, notwithstanding the locally high value of Re_λ, especially since both these effects are known to induce strong departures from LI. In fact, a large percentage of the ASL data in figure 8(*a*) were obtained by Wyngaard & Tennekes (1970) at three heights ($z = 5.66$, 11.3 and 22.6 m) above the ground (no information for the stability conditions is given). Under 'neutral' conditions, the ASL should be comparable (at similar values of z/δ) with the laboratory boundary layer provided the nature of the surface is comparable. It is difficult to estimate with confidence the thickness δ of the neutral ASL. Wyngaard (2010) suggests that, under neutral conditions, δ may scale with U_τ/f (U_τ is the friction velocity and f is the Coriolis parameter) and estimates, for mid-latitudes, δ to be within the range 250 to 2500 m. This implies that the majority of the neutral ASL data for F were taken in the region $z/\delta < 0.1$. It is not difficult to conclude that there is quite a lot of uncertainty in the estimation of δ, e.g. a value of δ smaller than 100 m was found by Metzger, McKeon & Holmes (2007) based on experiments in Utah's western desert for almost 'exactly' neutral conditions; the authors stressed, however, the difficulties associated in making measurements under those conditions. In any case, it is not clear if any of the published ASL data were obtained under 'exactly' neutral conditions. Certainly, it is unwise to assume that the measurements of F in region $z/\delta < 0.1$ have not been affected by the proximity to the surface.

Recent measurements (Djenidi *et al.* 2017*c*) in a laboratory boundary layer over smooth and rough walls indicate that the magnitude of F can increase, perhaps by as much as a factor of 3, in the region $z/\delta < 0.1$. For the ASL data in figure 8(*a*) of Sreenivasan & Antonia (1997), it is almost certain that F was invariably estimated over a range of heights that would correspond to the inner region of the laboratory

https://doi.org/10.1017/jfm.2018.307 Published online by Cambridge University Press

boundary layer. For example, for the nearly neutral ASL data measured by Gibson *et al.* (1970) above the ocean surface, F is in the range 13 to 26 (the height is in the range 2.25 m to 12.25 m); this variation is typical of that found in the inner region of the laboratory boundary layer (Djenidi *et al.* 2017*c*). Further, one should also check that there are no major departures from LI in this range due to the probable effect of the mean shear. In the region $z/\delta < 0.1$, a larger departure from LI is expected due to the combined effect of an increase in mean shear and the presence of the surface. Clearly, the use of F in the first few metres of the ASL has misled a vast majority of researchers into preferring K62 over K41. More importantly, when the ASL data are disregarded, the (laboratory) data in figure 8(*b*) are consistent with the trend displayed in figures 4, 6 and 7, providing further strong support that F increases as Re_λ increases, eventually becoming constant when Re_λ is sufficiently large. Note that the log–log scale in figure 8(*a*), together with the weighting of the ASL data, have 'aided and abetted' the support for a power-law dependence of F on Re_λ.

4. Conclusions and final discussion

An analytical expression for the flatness factor F in HIT has been derived by applying the limit at small separation to the transport equation for $\overline{(\delta u)^3}$. The FRN effect, due to the influence of the large-scale motion, can be recast in the form $\beta S_3/Re_\lambda$ (2.16). This is of similar form to the FRN effect on S_3, i.e. C/Re_λ in (1.4). The analysis is developed solely by assuming local homogeneity and isotropy. The final expression for F indicates that this quantity, which is often used as a measure of intermittency, is balanced mostly by the pressure diffusion of energy, viscous destructive effects and large-scale effects (decay and/or production). We have estimated that the viscous destructive effect is negligible at moderate values of Re_λ. Since the large-scale effect decreases as Re_λ^{-1}, F is expected to be balanced solely by the correlation $\overline{(\partial u^*/\partial x^*)^2(\partial^2 p^*/\partial x^{*2})}$, thus emphasizing the role of the pressure fluctuation in limiting the growth of intermittency, as measured by F. This correlation is expected to become constant at sufficiently large Re_λ. A possible physical interpretation of (2.15) is as follows. Enhanced local vortex stretching leads to an increased concentration of turbulent fluctuations in reduced regions of space. This results in an increased intermittency as reflected in the skewness and, more markedly, the flatness factor. The pressure diffusion term, which accounts for non-local interactions (reflected by the contributions of all wavenumbers to the integral in (2.18)), acts to slow down the rate at which the intermittency increases with Re_λ whilst viscous effects (through the term G/Re_λ in (1.4)) account for the destruction of the skewness S_3. Speculatively it would appear that the pressure diffusion effect in (2.15) is not as effective as the viscous destruction term of S_3 so that F tends to a constant at larger values of Re_λ than S_3. DNS results for $\overline{(\partial u^*/\partial x^*)^2(\partial^2 p^*/\partial x^{*2})}$, in both forced turbulence and other turbulent flows, are needed to confirm this speculation.

The variation of F with Re_λ has been examined in various turbulent flows: on the axis in the far field of plane and circular jets, grid turbulence, SFPBT, along the centreline of wakes, a fully developed channel flow, and the flow of helium gas at low temperature between two counter-rotating disks. In particular, we reinterpret this variation in the light of the FRN effect (Antonia *et al.* 2017). Figures 3 and 4 show clearly that, at relatively low Re_λ, F can differ from flow to flow and, for a given flow, it may also depend on the initial conditions. This FRN effect on F is further highlighted by applying least-square fits, using (2.16), to the circular jet and plane jet

https://doi.org/10.1017/jfm.2018.307 Published online by Cambridge University Press

data (see figure 4); it strongly supports the notion that F is affected by the FRN effect differently in different flows. The magnitude of F in various flows (figures 4, 6 and 7), e.g. in grid turbulence, and along the axes in the far field of plane and circular jets, increases as Re_λ increases, and appears to approach a constant, with a value slightly larger than 10, when Re_λ is sufficiently large. This trend is consistent with all the laboratory data for F examined by Sreenivasan & Antonia (1997). More importantly, if we ignore the ASL data, all the laboratory data for F seem consistent with K41, at least when Re_λ approaches 10^3, in the sense that F approaches a constant value; this is also consistent with the analysis of § 2. It is also consistent with the closure theory of intermittency, based on a variational approach, by Qian (1986). His computational results showed that F has an upper bound ($\approx$15) when Re_λ is sufficiently large ($\approx 10^5$). The same variational approach was used by Qian (1983) to derive the $k^{-5/3}$ law, thus lending credence to his claim that K41 cannot be ruled out merely because ϵ fluctuates. Whilst the trend of F towards a constant at sufficiently large Re_λ is adequately supported by all the data examined in this paper, it is premature to claim that the 'constant' value reached by F is universal, i.e. flow-independent. Evidently, more high-quality data for the variation of F on Re_λ, preferably for Re_λ in excess of 1000, are required in different flows, or flow regions where the departure from local isotropy is minimal. The present analytical work, supplemented by what we believe to be a more realistic approach for investigating the dependence of F versus Re_λ, should provide sufficient stimulus to numericists, using simulations either of the DNS type or the eddy-damped quasi-normal Markovian (EDQNM) approach, to confirm the tendency of F towards a constant at large Re_λ.

Acknowledgements

S.L.T. wishes to acknowledge support given to him from the NSFC through grant 11702074. Y.Z. wishes to acknowledge support given to him from the Research Grants Council of Shenzhen Government through grant JCYJ20150625142543469 and the NSFC through grant 11632006. L.D. thanks the LabEx EMC3, as well as FEDER, for financial support.

REFERENCES

ANTONIA, R. A., ANSELMET, F. & CHAMBERS, A. J. 1986 Assessment of local isotropy using measurements in a turbulent plane jet. *J. Fluid Mech.* **163**, 365–391.

ANTONIA, R. A., CHAMBERS, A. J. & SATYAPRAKASH, B. R. 1981 Reynolds number dependence of high-order moments of the streamwise turbulent velocity derivative. *Boundary-Layer Meteorol.* **21**, 159–171.

ANTONIA, R. A., DJENIDI, L. & DANAILA, L. 2014 Collapse of the turbulent dissipation range on Kolmogorov scales. *Phys. Fluids* **26**, 045105.

ANTONIA, R. A., DJENIDI, L., DANAILA, L. & TANG, S. L. 2017 Small scale turbulence and the finite Reynolds number effect. *Phys. Fluids* **29** (2), 020715.

ANTONIA, R. A., SATYAPRAKASH, B. R. & HUSSAIN, A. K. M. F. 1982 Statistics of fine-scale velocity in turbulent plane and circular jets. *J. Fluid Mech.* **119**, 55–89.

ANTONIA, R. A., TANG, S. L., DJENIDI, L. & DANAILA, L. 2015 Boundedness of the velocity derivative skewness in various turbulent flows. *J. Fluid Mech.* **781**, 727–744.

ANTONIA, R. A., ZHOU, T. & ROMANO, G. P. 2002 Small-scale turbulence characteristics of two-dimensional bluff body wakes. *J. Fluid Mech.* **459**, 67–92.

BATCHELOR, G. K. & TOWNSEND, A. A. 1947 Decay of vorticity in isotropic turbulence. *Proc. R. Soc. Lond.* A **190**, 534–550.

https://doi.org/10.1017/jfm.2018.307 Published online by Cambridge University Press

BATCHELOR, G. K. & TOWNSEND, A. A. 1949 The nature of turbulent motion at large wave-numbers. *Proc. R. Soc. Lond.* A **199**, 238–255.

BELIN, F., MAURER, J., TABELING, P. & WILLAIME, H. 1997 Velocity gradient distributions in fully developed turbulence: experimental study. *Phys. Fluids* **9**, 3843–3850.

BURATTINI, P., LAVOIE, P. & ANTONIA, R. A. 2008 Velocity derivative skewness in isotropic turbulence and its measurement with hot wires. *Exp. Fluids* **45**, 523–535.

DAVIDSON, P. A. 2004 *Turbulence: An Introduction for Scientists and Engineers*. Oxford University Press.

DIMOTAKIS, P. E. 2000 The mixing transition in turbulent flows. *J. Fluid Mech.* **409**, 69–98.

DJENIDI, L., ANTONIA, R. A. & DANAILA, L. 2017*a* Self-preservation relation to the Kolmogorov similarity hypotheses. *Phys. Rev. Fluids* **2**, 054606.

DJENIDI, L., ANTONIA, R. A., DANAILA, L. & TANG, S. L. 2017*b* A note on the velocity derivative flatness factor in decaying HIT. *Phys. Fluids* **29**, 051702.

DJENIDI, L., ANTONIA, R. A., TALLURU, M. K. & ABE, H. 2017*c* Skewness and flatness factors of the longitudinal velocity derivative in wall-bounded flows. *Phys. Rev. Fluids* **2**, 064608.

FRIEHE, C. A., VAN ATTA, C. W. & GIBSON, C. H. 1971 Jet turbulence: dissipation rate measurements and correlations. *AGARD Turbul. Shear Flows* **18**, 1–7.

GAUDING, M. 2014 Statistics and scaling laws of turbulent scalar mixing at high Reynolds numbers. PhD thesis, RWTH Aachen University.

GIBSON, C. H., STEGEN, G. R. & WILLIAMS, R. B. 1970 Statistics of the fine structure of turbulent velocity and temperature fields at high Reynolds number. *J. Fluid Mech.* **41**, 153–167.

GOTOH, T., FUKAYAMA, D. & NAKANO, T. 2002 Velocity field statistics in homogeneous steady turbulence obtained using a high-resolution direct numerical simulation. *Phys. Fluids* **14**, 1065–1081.

GOTOH, T. & NAKANO, T. 2003 Role of pressure in turbulence. *J. Stat. Phys.* **113**, 855–874.

GYLFASON, A., AYYALASOMAYAJULA, S. & WARHAFT, Z. 2004 Intermittency, pressure and acceleration statistics from hot-wire measurements in wind-tunnel turbulence. *J. Fluid Mech.* **501**, 213–229.

HILL, R. J. 2001 Equations relating structure functions of all orders. *J. Fluid Mech.* **434**, 379–388.

HILL, R. J. 2002 Scaling of acceleration in locally isotropic turbulence. *J. Fluid Mech.* **452**, 361–370.

ISHIHARA, T., GOTOH, T. & KANEDA, Y. 2009 Study of high-Reynolds number isotropic turbulence by direct numerical simulation. *Annu. Rev. Fluid Mech.* **41**, 165–180.

ISHIHARA, T., KANEDA, Y., YOKOKAWA, M., ITAKURA, K. & UNO, A. 2003 Spectra of energy dissipation, enstrophy and pressure by high-resolution direct numerical simulations of turbulence in a periodic box. *J. Phys. Soc. Japan* **72**, 983–986.

ISHIHARA, T., KANEDA, Y., YOKOKAWA, M., ITAKURA, K. & UNO, A. 2007 Small-scale statistics in high-resolution direct numerical simulation of turbulence: Reynolds number dependence of one-point velocity gradient statistics. *J. Fluid Mech.* **592**, 335–366.

JIMENEZ, J., WRAY, A. A., SAFFMAN, P. G. & ROGALLO, R. S. 1993 The structure of intense vorticity in isotropic turbulence. *J. Fluid Mech.* **255**, 65–90.

KAHALERRAS, H., MALECOT, Y. & GAGNE, Y. 1998 Intermittency and Reynolds number. *Phys. Fluids* **10**, 910–921.

KERR, R. M. 1985 Higher-order derivative correlations and the alignment of small-scale structures in isotropic numerical turbulence. *J. Fluid Mech.* **153**, 31–58.

KIM, J. & ANTONIA, R. A. 1993 Isotropy of the small-scales of turbulence at small Reynolds numbers. *J. Fluid Mech.* **251**, 219–238.

KOLMOGOROV, A. N. 1941*a* Dissipation of energy in the locally isotropic turbulence. *Dokl. Akad. Nauk SSSR* **32**, 19–21.

KOLMOGOROV, A. N. 1941*b* Local structure of turbulence in an incompressible fluid for very large Reynolds numbers. *Dokl. Akad. Nauk SSSR* **30**, 299–303.

KOLMOGOROV, A. N. 1962 A refinement of previous hypotheses concerning the local structure of turbulence in a viscous incompressible fluid at high Reynolds number. *J. Fluid Mech.* **13**, 82–85.

https://doi.org/10.1017/jfm.2018.307 Published online by Cambridge University Press

KRAICHNAN, R. H. 1991 Turbulent cascade and intermittency growth. *Proc. R. Soc. Lond.* A **434**, 65–78.

KUO, A. Y.-S. & CORRSIN, S. 1971 Experiments on internal intermittency and fine-structure distribution functions in fully turbulent fluid. *J. Fluid Mech.* **50** (02), 285–319.

METZGER, M., MCKEON, B. J. & HOLMES, H. 2007 The near-neutral atmospheric surface layer: turbulence and non-stationarity. *Phil. Trans. R. Soc. Lond.* A **365**, 859–876.

MI, J., XU, M. & ZHOU, T. 2013 Reynolds number influence on statistical behaviors of turbulence in a circular free jet. *Phys. Fluids* **25**, 075101.

MOISY, F., TABELING, P. & WILLAIME, H. 1999 Kolmogorov equation in a fully developed turbulence experiment. *Phys. Rev. Lett.* **82** (20), 3994–3997.

MYDLARSKI, L. & WARHAFT, Z. 1996 On the onset of high-Reynolds-number grid-generated wind tunnel turbulence. *J. Fluid Mech.* **320**, 331–368.

PEARSON, B. R. & ANTONIA, R. A. 2001 Reynolds-number dependence of turbulent velocity and pressure increments. *J. Fluid Mech.* **444**, 343–382.

PEARSON, B. R. & KROGSTAD, P. A. 2001 Further evidence for a transition in small-scale turbulence. In *14th Australasian Fluid Mechanics Conference, Adelaide*.

QIAN, J. 1983 Variational approach to the closure problem of turbulence theory. *Phys. Fluids* **26** (8), 2098–2104.

QIAN, J. 1986 A closure theory of intermittency of turbulence. *Phys. Fluids* **29**, 2165.

SADDOUGHI, S. G. & VEERAVALLI, S. V. 1994 Local isotropy of turbulent boundary layers at high Reynolds number. *J. Fluid Mech.* **268**, 333–372.

SHEN, X. & WARHAFT, Z. 2000 The anisotropy of the small scale structure in high Reynolds number ($R_\lambda \sim 1000$) turbulent shear flow. *Phys. Fluids* **12**, 2976–2989.

SINHUBER, M., BODENSCHATZ, E. & BEWLEY, G. P. 2015 Decay of turbulence at high Reynolds numbers. *Phys. Rev. Lett.* **114** (3), 034501.

SREENIVASAN, K. & ANTONIA, R. A. 1997 The phenomenology of small-scale turbulence. *Annu. Rev. Fluid Mech.* **29**, 435–472.

SREENIVASAN, K. R. 1995 Small-scale intermittency in turbulence. In *Proc. Twelfth Australasian Fluid Mechanics Conference, University of Sydney, Australia*, pp. 549–556.

TABELING, P. & WILLAIME, H. 2002 Transition at dissipative scales in large Reynolds number turbulence. *Phys. Rev.* E **65**, 066301.

TABELING, P., ZOCCHI, G., BELIN, F., MAURER, J. & WILLAIME, H. 1996 Probability density functions, skewness, and flatness in large Reynolds number turbulence. *Phys. Rev.* E **53**, 1613–1621.

TANG, S. L., ANTONIA, R. A., DANAILA, L., DJENIDI, L., ZHOU, T. & ZHOU, Y. 2016 Towards local isotropy of higher-order statistics in the intermediate wake. *Exp. Fluids* **57**, 111.

TANG, S. L., ANTONIA, R. A., DJENIDI, L., ABE, H., ZHOU, T., DANAILA, L. & ZHOU, Y. 2015*a* Transport equation for the mean turbulent energy dissipation rate on the centreline of a fully developed channel flow. *J. Fluid Mech.* **777**, 151–177.

TANG, S. L., ANTONIA, R. A., DJENIDI, L. & ZHOU, Y. 2015*b* Transport equation for the isotropic turbulent energy dissipation rate in the far-wake of a circular cylinder. *J. Fluid Mech.* **784**, 109–129.

THIESSET, F., ANTONIA, R. A. & DJENIDI, L. 2014 Consequences of self-preservation on the axis of a turbulent round jet. *J. Fluid Mech.* **748**, R2.

THIESSET, F., DANAILA, L. & ANTONIA, R. A. 2013 Dynamical effect of the total strain induced by the coherent motion on local isotropy in a wake. *J. Fluid Mech.* **720**, 393–423.

TONG, C. & WARHAFT, Z. 1994 On passive scalar derivative statistics in grid turbulence. *Phys. Fluids* **6** (6), 2165–2176.

VAN ATTA, C. W. & ANTONIA, R. A. 1980 Reynolds number dependence of skewness and flatness factors of turbulent velocity derivatives. *Phys. Fluids* **23**, 252–257.

WANG, L.-P., CHEN, S., BRASSEUR, J. G. & WYNGAARD, J. C. 1996 Examination of hypotheses in Kolmogorov refined turbulence theory through high-resolution simulations. Part 1. Velocity field. *J. Fluid Mech.* **309**, 113–156.

WYNGAARD, J. C. 2010 *Turbulence in the Atmosphere*. Cambridge University Press.

https://doi.org/10.1017/jfm.2018.307 Published online by Cambridge University Press

WYNGAARD, J. C. & TENNEKES, H. 1970 Measurements of the small-scale structure of turbulence at moderate Reynolds numbers. *Phys. Fluids* **13**, 1962–1969.

XU, G., ANTONIA, R. A. & RAJAGOPALAN, S. 2001 Sweeping decorrelation hypothesis in a turbulent round jet. *Fluid Dyn. Res.* **28** (5), 311–321.

YEUNG, P. K., DONZIS, D. A. & SREENIVASAN, K. R. 2005 High-Reynolds-number simulation of turbulent mixing. *Phys. Fluids* **17**, 081703.

YEUNG, P. K. & ZHOU, Y. 1997 Universality of the Kolmogorov constant in numerical simulations of turbulence. *Phys. Rev.* E **56**, 1746–1752.

ZHOU, T. & ANTONIA, R. A. 2000 Reynolds number dependence of the small-scale structure of grid turbulence. *J. Fluid Mech.* **406**, 81–107.

ZHOU, T., ANTONIA, R. A. & CHUA, L. P. 2005 Flow and Reynolds number dependencies of one-dimensional vorticity fluctuations. *J. Turbul.* **6**, N28.

https://doi.org/10.1017/jfm.2018.307 Published online by Cambridge University Press